Journal of CO2 Utilization xxx (xxxx) 101719

Contents lists available at ScienceDirect

Journal of CO2 Utilization

journal homepage: www.elsevier.com/locate/jcou

Modeling the time evolution of the dissociation fraction in low-pressure CO_2 plasmas

Tiago Silva [a], Ana Sofia Morillo-Candas [b], Olivier Guaitella [b], Vasco Guerra [a,*]

[a] Instituto de Plasmas e Fusão Nuclear, Instituto Superior Técnico, Universidade de Lisboa, Portugal
[b] Laboratoire de Physique des Plasmas (UMR 7648), CNRS-Univ Paris Sud-Sorbonne Univesité-École polytechnique, F-91128, Palaiseau, France

ARTICLE INFO

Keywords:
Plasma
CO_2 dissociation
Electronically excited metastable
Modelling
Time evolution

ABSTRACT

The time evolution of the CO_2 dissociation fraction in pulsed discharges is studied through kinetic modeling. The simulations are compared against experimental data obtained in pulsed DC glow and radio-frequency discharges, operated with currents of about 40 mA and powers of 40 W, sustained under low gas pressures (< 600 Pa). The model is used to analyse the experimental trends associated with different pulsed configurations, namely different combinations of pulse duration and delay between pulses. The results validate the chemical module used in this work and reveal the importance of electronically excited states, in particular $CO(a^3\Pi)$, to describe the evolution of $CO_2(X^1\Sigma^+)$ and $CO(X^1\Sigma_g^+)$ densities. In particular, it is shown that $CO(a^3\Pi)$ can promote CO_2 formation for increasing concentrations of O_2 due to bimolecular reactions such as $CO(a^3\Pi) + O_2(X^3\Sigma_g^-) \rightarrow CO_2(X^1\Sigma^+) + O(^3P)$. At the same time, for low concentration of O_2 the CO_2 dissociation fraction can be stimulated through $CO(a^3\Pi) + CO_2(X^1\Sigma^+) \rightarrow 2CO(X^1\Sigma_g^+) + O(^3P)$. It is also found that the pulse parameters influence the concentration of $O_2(X^3\Sigma_g^-)$ by favouring or limiting oxygen atomic recombination during the afterglow. Overall, this work addresses reaction mechanisms often overlooked in the CO_2 plasma-based reforming literature, while confirming that electronically excited states play a key role in describing the dissociation fraction in CO_2 plasmas operated under low pressure conditions.

1. Introduction

The goal of zero net emissions by 2050 [1] requires new technologies capable of solving the unpredictable nature of renewable energy sources. One promising and environmentally friendly solution relies on CO_2 recycling towards high-energy-density chemicals, using the excess of renewable power along the transformation process [2]. To this purpose, plasma technology has gained much attention due to its potential to activate CO_2 at reduced energy cost while exciting molecular vibrations to overcome the dissociation barrier [3]. Combining plasma reactors with an efficient reduction of CO_2 would allow the conversion of electricity into chemical potential energy, leading to the decarbonization of energy sectors and the production of fuels in remote locations where renewable energy access is optimal [4]. Several research groups are currently investigating what can be the maximally achievable energy efficiency associated with the CO_2 plasma-based reduction. Some recent experimental studies are based on: (i) thermally driven dissociation, using high-power microwave discharges that significantly heat the background gas in the range of 2000–4000 K [5], (ii) nanosecond repetitively pulsed discharges, using different plasma pulse sequences to improve the conversion [6], (iii) dielectric barrier discharges, combining the gas flow with sorbents to induce CO_2 capture and conversion [7] and (iv) arc plasma technology with optimized geometry to enhance conversion process [8]. Many other research works are discussed in recent reviews related to the topic of CO_2 plasma-based reduction (see e.g. [9,10]).

Despite recent progress on this research topic, plasma applications for large-scale fuel production are not yet viable and many important challenges remain to be solved. First, the role of vibrational excitation and thermal mechanisms of CO_2 dissociation still need to be clarified. To the best of our knowledge, the energy efficiency values of about 90 % obtained through supersonic gas flow conditions claimed in [3] remain to be experimentally reproduced. Such high energy-efficiency values require an optimized transfer of electron energy towards CO_2 vibrations and appropriate control of the gas dynamics [11]. The highest energy efficiency values recently reported are around 50–60 % [9]. Second, further research is required in the domain of CO_2 conversion through power modulation and plasma catalysis. Investigation needs to

* Corresponding author.
E-mail address: vguerra@tecnico.ulisboa.pt (V. Guerra).

https://doi.org/10.1016/j.jcou.2021.101719
Received 19 July 2021; Received in revised form 9 September 2021; Accepted 12 September 2021

progress towards a better understanding of pulsing optimization for CO_2 conversion, while investigating new catalyst activation methods [12]. Finally, and given the necessity to separate decomposition products from the initial CO_2 mixture, research also needs to advance towards the development of separation processes, specifically designed to plasma technology applications. In relation to this topic, there is an increasing interest on mixed ion electron conducting membranes [13] and plasma electrochemical interaction using solid oxide cell technology [14]. Understanding the synergy between the plasma and the membrane surface to optimize operating temperatures and conversion ratios remains an open challenge and is a priority on the way to reach economic goals [15].

In addition to experimental studies, the scaling of laboratory processes towards industrial scales requires comprehensive numerical modeling, specifically dedicated to the study of the CO_2 plasma chemistry. The N-PRiME group in Lisbon has been actively contributing to this effort. In particular, and given the necessity to describe various plasma kinetics of CO_2 plasmas and CO_2 conversion under different experimental conditions, previous modelling research works were focused on: (i) electron-neutral scattering cross sections for CO_2 [16] and CO [17], (ii) relaxation of CO_2 vibrationally excited levels [18] (iii) transfer of electron energy towards CO_2 vibrations [19] (iv) influence of N_2 on the CO_2 dissociation yield and vibrational distribution functions [20], (v) gas heating in the afterglow of pulsed CO_2 discharges [21], (vi) reaction mechanisms responsible for the formation of CO_2 dissociation products [22] and (vii) CO_2 dissociation under Martian environment for oxygen production [23,24]. These efforts were always accompanied by comparison of the modelling results against experimental data obtained by research groups in Paris and Eindhoven, using DC glow discharges (plasmas sustained by high voltages inside a pair of electrodes) and advanced plasma diagnostics, namely Fourier Transform infra-red absorption spectroscopy [25] and optical emission spectroscopy [26]. Despite the low energy efficiency and moderately low CO_2 dissociation fraction values typically associated with DC glow discharges, these plasma sources constitute ideal systems for fundamental studies given their simple geometry and homogeneity of its positive column. These features facilitate the study of CO_2 plasmas through the use of volume average 0D self-consistent kinetic models to account for its very complex kinetics.

This paper presents a modelling investigation aimed at studying the influence of electronically excited states on the dissociation fraction of CO_2 plasmas. While the contribution of vibrationally excited CO_2 to the dissociation fraction has been largely discussed in literature (see e.g. [27–29]), the role of electronically excited states is often overlooked. These states can play an important role in the kinetics of CO_2 discharges under low-pressure conditions or when electronic excitation is the dominant mechanism of dissociation due to high values of reduced electric fields (see e.g. [30,31]). The modelling results are compared against experimental data obtained in the so-called building-up experiments [32,33]. These experiments, performed under static conditions (no gas flow), are particularly relevant to investigate the influence of heavy particle reactions on CO_2 conversion. Capitalizing on these experimental studies, we develop a model to simulate pulsed CO_2 discharges and quantify the role of electronic excited states. The next section details the experimental campaign, along with a short summary and description of the main experimental results and trends found. The third section provides an overview of the plasma model and approximations considered. We present modelling results obtained under continuous plasma operation and discuss the creation and loss mechanisms that lead to the formation of various species in the plasma. In the fourth section, we compare modeling results against experimental data obtained in building-up experiments, while discussing and interpreting the model assumptions to describe the CO_2 dissociation fraction and the different trends related to different pulse parameters. The concluding remarks are given in section 5.

2. Brief overview of the building-up experiment

Building-up experiments were performed in CO_2 pulsed DC glow discharges [32] and pulsed capacitively-coupled radio frequency discharges [33], and consisted of consecutive trains of plasma pulses, sustained under static conditions with a closed reactor and without gas flow. These features enable to remove the influence of the residence time while studying the influence of processes with different characteristic times during the active phase and afterglow of the plasma pulse. Gas pressures were typically varied between 133.3 and 666.6 Pa (1 and 5 Torr), while currents ranged from 20 to 40 mA in the case of pulsed DC glow discharges and powers were varied between 40 and 80 W in the case of the pulsed capacitively-coupled radio frequency discharges. Both discharges were ignited in cylindrical Pyrex tubes with 2 cm inner diameter and 23 cm length. The time evolution of the rotational/vibrational temperatures and species concentrations were monitored during the plasma pulses with a Fourier Transform infra-red (FTIR) spectrometer (Bruker, Vertex 70) with a spectral resolution of 0.2 cm^{-1}. Special attention was given to the measurement of the CO_2 dissociation fraction, represented by the parameter α:

$$\alpha = \frac{[CO]}{[CO] + [CO_2]} \quad (1)$$

where $[CO]$ and $[CO_2]$ are the gas phase concentrations of CO and CO_2, respectively. More details about the experimental setup, procedure and plasma diagnostics used can be found in the original experimental references [32,33].

2.1. Notation

Trains of plasma pulses in the building-up experiments [32,33] are defined by the total number of trains (N_{tr}), the number of pulses per train (N_p), the pulse duration ON time (t_p^{ON}) and the delay between consecutive plasma pulses (t_p^{OFF}). From these quantities, we can define the total plasma ON time per train of plasma pulses, i.e., $t_{tr}^{ON} = N_p \cdot t_p^{ON}$, the total plasma OFF time per train of plasma pulses, $t_{tr}^{OFF} = N_p \cdot t_p^{OFF}$ and the total plasma ON time in the experiment, $T^{ON} = N_{tr} \cdot t_{tr}^{ON}$. These quantities are schematically represented in Fig. 1. Typical series of plasma pulses with a total number of trains $N_{tr} = 500$ lead to a total experiment time of around 17 min for each condition. Note that after every train of plasma pulses an infrared absorption measurement is acquired with the gas in thermal equilibrium. The total measurement time is 2 s. This value includes the time the FTIR waits for the ignition of the train of plasma pulses and the time required by the mirror of the FTIR to scan the whole wavelength range.

2.2. Overview of the main results

The measurements in the building up experiments [32,33] revealed the following general trend for the CO_2 dissociation fraction: linear evo-

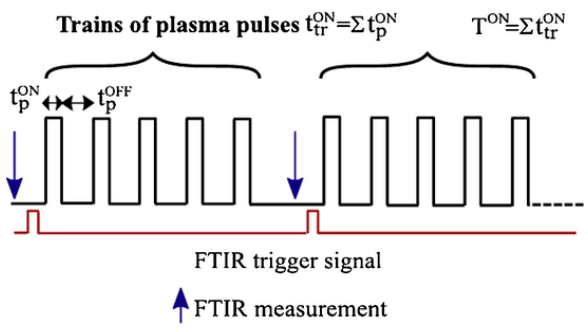

Fig. 1. Generic pulse plasma diagram used during the FTIR measurement in the building-up experiments.

lution with the plasma ON time T^{ON} until about 0.5–1 s, followed by a steady-state equilibrium (plateau) towards long plasma ON times. Fig. 2 shows typical results of the dissociation fraction, experimentally obtained in pulsed DC glow discharge for different pressure values (133.3 and 533.3 Pa) with a discharge current of 40 mA. In this example, the train configuration consists of 10 pulses per train (N_p = 10) leading to a total plasma ON per train of 50 ms, and after 500 trains to a total plasma ON time of 25 s. The change of the dissociation fraction with the pressure observed in Fig. 2 is deeply related to the value of the reduced electric field E/N, i.e., electric field over the gas density. Note that the reduced electric field decreases significantly with the gas pressure. Consequently, and given the strong contribution of electron impact dissociation at short plasma ON times, the initial growth of the dissociation fraction becomes faster as the pressure decreases. The validity of the electron impact dissociation cross section by Polak and Slovetsky (see e.g. [16]) could be established in reference [19] in the range of reduced electric field of ~ 45–110 T d. Nevertheless, a recent study suggests that for higher reduced electric field values, the cross section Polak and Slovetsky may underestimate the conversion efficiency [34]. Note that different values of reduced electric fields can stimulate different CO_2 decomposition channels (see [16] for more details). The cross section leading to $O(^1D)$ and $CO(X^1\Sigma_g^+)$, which dominates for lower reduced electric fields, might be better established than the cross section responsible for the creation of $CO(a^3\Pi)$ and $O(^3P)$, which becomes more relevant at large reduced electric fields. Finding a suitable cross section, capable to describe electron-impact CO_2 dissociation over low and high range of reduced electric fields, still requires future investigations.

In this paper, we are interested at describing the time evolution of plasma species, the relative importance of different mechanisms and the experimental trends associated with the changes of the dissociation fraction due to modifications of pulse-related parameters, namely pulse frequency and duration within the train of plasma pulses. In other words, we intend to study multipulse conditions associated with different configurations of series of trains of plasma pulses, while keeping the gas pressure and discharge power/current constants. According to the experimental results obtained in [33] these conditions should provide roughly the same dissociation fraction slope for short plasma ON times, while the steady-state dissociation fraction value can vary according to the pulse configuration. Considering that these variations occur at long plasma ON times, we expect a strong role of recombination mechanisms at describing the dissociation fraction values.

In summary, the following results and trends were observed throughout the multipulse experiments [32,33]:

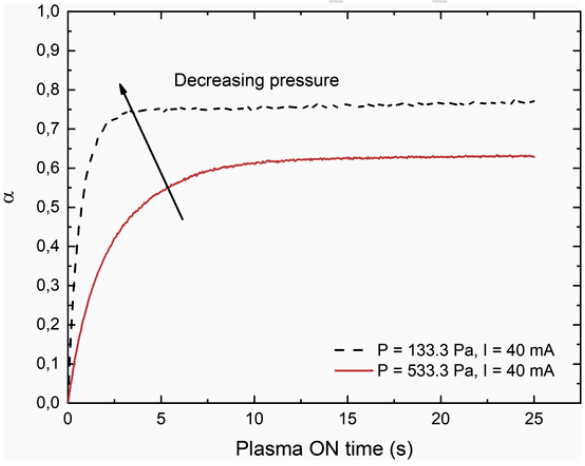

Fig. 2. Time evolution of the dissociation fraction measured in a DC glow discharge, for two pressures (133.3 and 533.3 Pa) and discharge current of 40 mA.

1. the steady-state dissociation fraction in continuous plasma is larger than that in the pulsed plasmas;
2. the time T^{ON} at which the dissociation fraction curves diverge due to pulse variations is within the range 0.5–1 s;
3. the increase of the off-time delay (t_p^{OFF}) leads to the decrease of the dissociation fraction at steady-state;
4. the increase of the number of pulses per train (N_p), keeping the same pulse duration (t_p^{ON}) and off-time delay (t_p^{OFF}), leads to an increase of the dissociation fraction at steady state.
5. the increase of the pulse duration (t_p^{ON}) leads to a significant increase of the dissociation fraction at steady-state;

The previous points clearly suggest the occurrence of back-reactions that influence the CO_2 dissociation fraction at the steady-state region. In particular, and given the difference between continuous and pulsing experiments, they suggest the existence of chemical reactions that contribute for CO_2 recombination during the plasma OFF-time, as discussed in [33]. This outcome is surprising when considering that pulsing is often claimed to be beneficial for an efficient CO_2 dissociation. However, as mentioned in [33], this observation is only true if vibrational excitation plays an important role at dissociating CO_2 and there is no significant influence of back-reactions in the OFF phase of plasma pulse. The latter observation could suggest a decreasing contribution of three-body reaction mechanisms on CO_2 recombination during the OFF phase of the plasma pulse due to the decreasing gas temperatures. However, under the present experimental conditions, the results suggest that the recombination of CO_2 cannot be exclusively described by three-body reaction mechanisms with a positive gas temperature dependence.

3. Plasma model

To simulate the multipulse experiment, we developed a model targeted at describing the dissociation fraction of CO_2 as function of the plasma ON time for different pulse configurations, accounting for both t_p^{ON} and t_p^{OFF} phases. This requires a detailed description of the electron and heavy particle kinetics that influence the production and destruction of CO and CO_2 species. With regard to the electron kinetics, we relied on the Boltzmann solver (LoKI-B) [35,36] to calculate the electron energy distribution function (EEDF) as function of the reduced electric field. Electron-impact cross sections are taken from LXCat and described in [16] for CO_2, [17] for CO and [37,38] for oxygen species. For the input values of reduced electric field and electron density, we rely on the experimentally measured results and the simulations obtained in [22] for continuous DC glow discharges in CO_2. Note that we assume a constant value for the electron density and reduced electric field throughout the plasma pulse simulations. Although this approximation may lead to some inaccuracies in a full description of the physics of CO_2 discharges, it nevertheless enables one to analyse the contribution of heavy-particle reactions at the steady-state region and to describe the experimental trends associated with fixed values of pressure and current. The validity of this assumption is further discussed below for different conditions.

The evolution of heavy particles is described through the numerical solution of a system of balance equations according to:

$$\frac{\partial N_s}{\partial t} = \sum_i C_{s,i} - \sum_i D_{s,i} \quad (2)$$

where N_s, $C_{s,i}$ and $D_{s,i}$ are the density of species s and the rate of creation and loss of a given species in reaction i, respectively. Each heavy particle is then described by a set of creation and loss mechanisms that guarantee a steady state concentration at the end of the calculations and the conservation of oxygen and carbon atoms. Note that the model depends not only on input discharge parameters, namely gas pressure and gas temperature, but also time constraints related to the pulse configuration. Considering the necessity to accumulate pulses throughout

the calculations, the model takes into account the species concentrations at the end of the plasma pulses or at the end of the afterglows as inputs to calculate new concentrations during the next afterglow or the next discharge pulse, respectively, according to a specific pulse duration, off-time delay and number of pulses per train. In order to reproduce the experimental procedure of [32,33], we consider an OFF time in between consecutive trains of 2 s. The chemical module is based on the set proposed in [22], which includes various ground and electronic states of CO_2, CO, O_3, O_2 and O and C (see Table 1). This set has been extended with the inclusion CO_2 vibrational energy transfer mechanisms as described in [23]. Moreover, in this work we test the effect of additional chemical reactions involving electronically excited states of O and O_2 as described in section 3.1. It is also important to note that in this paper we do not consider any gas renewal given the absence of gas flow during the building-up experiments. In [22], at steady-state conditions, CO_2 was created mostly due to renewal of the gas entering the reactor, while CO was lost due to the flow of gas exiting the reactor. Due to the absence of gas flow, the dissociation fraction values at steady-state are expected to be higher than the ones found in [22] for similar conditions of pressure and current.

For the description of the heavy particles, two additional approximations are used throughout the calculations. First, we neglect the change of the electron-impact rate coefficients with the gas mixture, while considering the EEDF calculated in pure CO_2. Note that the CO_2 electron impact dissociation rate can change accordingly with the gas mixture. For instance, at about 80 Td (typical reduced electric field value obtained in [22]), the electron dissociation rate coefficient can change from roughly $1.3{\cdot}10^{-10}$ cm^3s^{-1} to about $8.5{\cdot}10^{-11}$ cm^3s^{-1} when the CO_2 dissociation fraction increases from 0 to 50 % (assuming that O_2 density is 2 times higher than the density of O atoms). Fig. 3 illustrates the EEDF calculated for two different values of dissociation fraction for a reduced electric field E/N = 80 Td. As discussed in detail in [17], the influence of the gas mixture on the electron dissociation rate coefficient can increase for lower reduced electric fields values. Taking into account the range of reduced electric fields explored in this work, we do not expect a significant influence of this approximation at describing the experimental trends associated to the changes of pulse parameters. For the conditions under study, the relative error in the calculated dissociation fraction associated with this approximation can be of about 7%. Second, we consider a distribution for the CO_2 vibrational levels with a temperature of 300 K when solving the Boltzmann equation to obtain the EEDF. Notice that superelastic collisions involving vibrational levels of CO_2 can slightly modify the electron energy distribution function, which modifies the electron dissociation rate coefficient (see e.g. [39]). At 80 Td, the electron dissociation rate coefficient can change from roughly $1.4{\cdot}10^{-10}$ cm^3s^{-1} to about $1.8{\cdot}10^{-10}$ cm^3s^{-1} when the vibrational temperature associated to asymmetric mode of CO_2 increases from 300 K to 1000 K (typical values measured in the experiment – see [33]). Considering these estimations and the relatively low vibrational excitation of our conditions, we assume that changes of the EEDF along each pulse are not very significant to describe the modifications observed at steady state due to different plasma pulsed parameters.

Table 1
List of the main neutral species (including ground and electronic excited states) considered in this work.

Species	Ground state	Excited electronic state
CO_2	CO_2 ($X^1\Sigma^+$)	–
O_2	O_2 ($X^3\Sigma_g^-$)	$O_2(a^1\Delta_g)$, $O_2(b^1\Sigma_g^+)$
O	O (^3P)	O (^1D)
CO	$CO(X^1\Sigma_g^+)$	$CO(a^3\Pi)$
O_3	$O_3(X^1A)$	O_3^*
C	$C(^3P)$	–

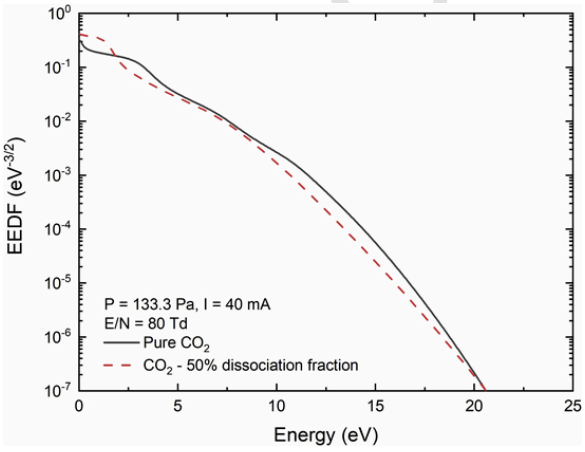

Fig. 3. EEDF obtained with gas pressure P = 133.3 Pa and discharge current of 40 mA.

3.1. Plasma active phase

The calculated time-dependent concentrations of the principal heavy particles produced as a result of CO_2 decomposition when a discharge is ignited from pure CO_2 are shown in Fig. 4. In this first example we consider a continuous plasma with a gas pressure P = 133.3 Pa, constant gas temperature T_g = 400 K, electron density $N_e = 7.02{\cdot}10^9$ cm^{-3} and a reduced electric field E/N = 81.5 Td (corresponding to an electron impact CO_2 dissociation rate of about $1.4{\cdot}10^{-10}$ cm^3s^{-1}). These input values are based on the simulation and experimental results obtained in [22] for a glow discharge sustained at 133.3 Pa with a current of 40 mA. The vertical dotted line in Fig. 4 refers to the typical time used as pulse duration in the building-up experiment (5 ms). Under these input conditions we can clearly see that all species reach steady-state at approximately 1 s. The $CO_2(X^1\Sigma^+)$ concentration starts decreasing around 0.1 s, while $CO(X^1\Sigma_g^+)$ becomes the dominant species. It is also worth noticing that at 5 ms the concentration of atomic oxygen O (^{3}P) is largely superior to $O_2(X^3\Sigma_g^-)$ given its direct production from O_2 ($X^3\Sigma_g^-$) dissociation and also quenching of O(^{1}D) (formed by direct dissociation of CO_2 ($X^1\Sigma^+$)) by the various plasma species. In relation to O_2 species, note that the concentrations of electronic excited O_2, namely the $O_2(a^1\Delta_g)$ state, also become relevant at the steady-state region.

The concentration of electronic excited state $CO(a^3\Pi)$ is relatively low at the steady-state region compared to the concentration of other

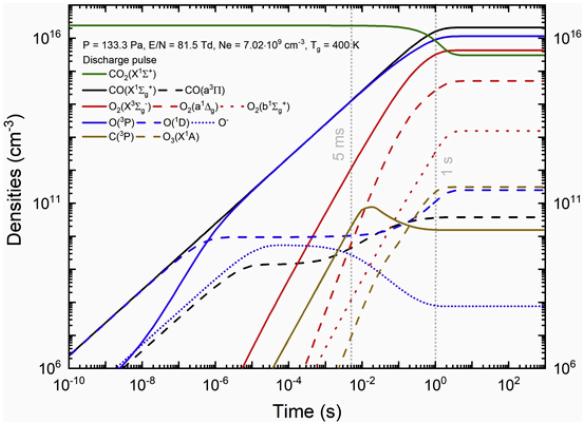

Fig. 4. Calculated concentration of the most important heavy particles as function of the discharge time, for gas pressure P = 133.3 Pa, gas temperature T_g = 400 K, electron density $N_e = 7.02{\cdot}10^9$ cm^{-3} and a reduced electric field E/N = 81.5 Td.

plasma species. Nevertheless, under the low-pressure conditions of this work, this state significantly influences the CO_2 dissociation fraction due to plasma-chemical reactions involving CO, O_2 and O species (see Fig. 5). Indeed, at steady-state, the concentrations of $CO(X^1\Sigma_g^+)$ and CO_2 $(X^1\Sigma^+)$ become strongly dependent on heavy-particles collisions involving $CO(a^3\Pi)$. The simulations show that the reaction $CO(a^3\Pi)$ + O_2 $(X^3\Sigma_g^-) \rightarrow CO_2$ $(X^1\Sigma^+)$ + O (^3P) contributes about 52 % to the production of CO_2 $(X^1\Sigma^+)$. This is followed by O- + $CO(X^1\Sigma_g^+) \rightarrow$ e + CO_2 $(X^1\Sigma^+)$ and $CO(a^3\Pi)$ + $CO(X^1\Sigma_g^+) \rightarrow CO_2$ $(X^1\Sigma^+)$ + $C(^3P)$ with contributions to the recombination of CO_2 $(X^1\Sigma^+)$ of about 23 % and 19 %, respectively. The second mechanism is somewhat surprising revealing the contribution of negative ions to the recombination into CO_2 $(X^1\Sigma^+)$. Indeed, to the best of our knowledge, there is a lack of studies in literature relating negative ions and the recombination of CO_2 in the context of plasma-based CO_2 reforming. Note that despite the low concentration of O- obtained at steady-state (about $7.6{\cdot}10^7$ cm^{-3} – see Fig. 4), the rate coefficient considered in this work for O- + $CO(X^1\Sigma_g^+) \rightarrow$ e + CO_2 $(X^1\Sigma^+)$ is rather high with $k(cm^3s^{-1}) = 5.8{\cdot}10^{-9}$ $Tg^{-0.39}$ according to [22]. The $CO(a^3\Pi)$ + $CO(X^1\Sigma_g^+) \rightarrow CO_2$ $(X^1\Sigma^+)$ + $C(^3P)$ mechanism is also particularly interesting as it represents a source of carbon atoms that should become significant for increasing concentrations of CO species. We consider that carbon atoms are mainly destroyed through recombination with O_2 species via $C(^3P)$ + O_2 $(X^3\Sigma_g^-) \rightarrow CO(X^1\Sigma_g^+)$ + O (^3P) with a constant rate coefficient of $3.0{\cdot}10^{-11}$ cm^3s^{-1} [22]. Finally, it is also worth emphasizing that the 3-body reactions mechanisms $(CO(X^1\Sigma_g^+)$ + $O(^3P)$ + M $\rightarrow CO_2(X^1\Sigma^+)$ + M) contribute only about 4% to the recombination of CO_2 $(X^1\Sigma^+)$ (see Fig. 5). This small contribution is expected given the low pressure (133.3 Pa) and relatively low gas temperature (400 K) considered in these simulations. Additional calculations with the same input conditions at 533.3 Pa show an increasing contribution of 3-body reactions to about 20 %.

With regard to $CO(X^1\Sigma_g^+)$ production, the reactions $CO(a^3\Pi)$ + O $(^3P) \rightarrow CO(X^1\Sigma_g^+)$ + O (^3P) and $CO(a^3\Pi)$ + $CO(X^1\Sigma_g^+) \rightarrow$ 2 $CO(X^1\Sigma_g^+)$ contribute about 57 % and 32 % at steady-state, respectively (see Fig. 5). Note, however, that these reactions do not constitute true production mechanisms of "CO molecules", as they just redistribute a fixed population among two CO electronic states. In relation to $CO(X^1\Sigma_g^+)$ production, it is also worth noticing that the reaction $CO(a^3\Pi)$ + CO_2 $(X^1\Sigma^+) \rightarrow 2CO(X^1\Sigma_g^+)$ + O (^3P), which does correspond to the creation of a CO molecule, can become relatively important at short times (< 1 s) given the high concentration of $CO_2(X^1\Sigma^+)$ and reduced values of the dissociation fraction. Its contribution decreases for longer times due to the decreasing concentration of $CO_2(X^1\Sigma^+)$ as result of $CO_2(X^1\Sigma^+)$ dissociation. Finally, with regard to loss mechanisms, it is worth mentioning that the reaction e + $CO(X^1\Sigma_g^+) \rightarrow$ e + $CO(a^3\Pi)$ greatly contributes to the destruction of $CO(X^1\Sigma_g^+)$, while the reaction

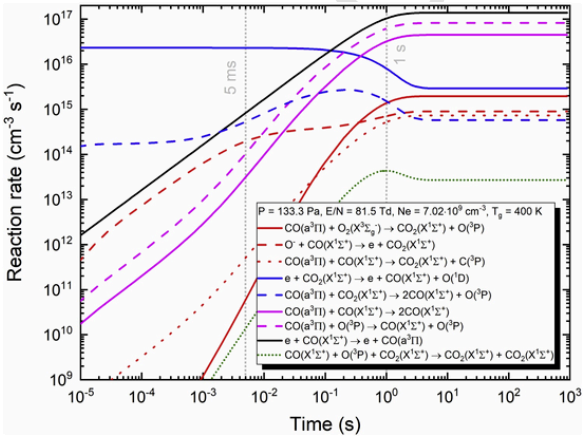

Fig. 5. Contributions of the main creation and loss mechanisms leading to the formation of CO_2 $(X^1\Sigma^+)$ and $CO(X^1\Sigma_g^+)$ for the same conditions used in Fig. 3.

e + CO_2 $(X^1\Sigma^+) \rightarrow CO(X^1\Sigma_g^+)$ + $O(^1D)$ plays a major role (74 %) to the destruction of CO_2 $(X^1\Sigma^+)$. Once more, the former reaction by itself does not destroy "CO molecules", but it opens a new energy transfer pathway that impacts the overall kinetics. The mechanism $CO(a^3\Pi)$ + CO_2 $(X^1\Sigma^+) \rightarrow 2CO(X^1\Sigma_g^+)$ + O (^3P) contributes about 15 % to the destruction of the CO_2 $(X^1\Sigma^+)$ at the steady-state region.

Overall, these results reveal the importance of reactions involving the $CO(a^3\Pi)$ state. Indeed, $CO(a^3\Pi)$ reactions are associated not only with the redistribution of the CO population among electronic states, but also the creation or destruction of CO and CO_2 molecules. The most relevant rate coefficients involving $CO(a^3\Pi)$ species, taken from [22] and used in this work are given in Tables 2 and 3. However, we should stress that the rate coefficients associated to these $CO(a^3\Pi)$ reactions exhibit significant discrepancies in literature (see e.g. [40,41]). As shown in section 4, changes in these rate coefficients can influence the dissociation fraction obtained at the steady state region and the dissociation fraction evolution along the discharge pulse. This point can only be clarified through experimental work or theoretical calculations dedicated to the assessment of rate coefficients involving the $CO(a^3\Pi)$ state. To further stress about the importance of $CO(a^3\Pi)$ in CO_2 plasmas, it should be noted that in nanosecond repetitively pulsed discharges (typically associated with high values of reduced electric field (> 100 Td)) $CO(a^3\Pi)$ can also affect the electron energy distribution function and transfer energy into the vibrations of $CO(X^1\Sigma_g^+)$ as discussed in [42]. Future studies dedicated to the improvement of our chemical module

Table 2
Set of main reactions that contribute to the creation of CO_2 $(X^1\Sigma^+)$ and $CO(X^1\Sigma_g^+)$. *f(E/N)* denotes an electron rate coefficient calculated from the Boltzmann equation.

State	Creation	Rate (cm^3/s), (cm^6/s)
$CO(X^1\Sigma_g^+)$	$CO(a^3\Pi)$ + $CO(X^1\Sigma_g^+) \rightarrow CO(X^1\Sigma_g^+)$ + $CO(X^1\Sigma_g^+)$	$5.6{\cdot}10^{-11}$
	$CO(a^3\Pi) + O(^3P) \rightarrow CO(X^1\Sigma_g^+) + O(^3P)$	$1.9{\cdot}10^{-10}$
	$CO(a^3\Pi) + O_2(X^3\Sigma_g^-) \rightarrow CO(X^1\Sigma_g^+) + O_2(X^3\Sigma_g^-)$	$2.4{\cdot}10^{-11}$
	$CO(a^3\Pi) + O_2(X^3\Sigma_g^-) \rightarrow CO(X^1\Sigma_g^+) + 2O(^3P)$	$2.4{\cdot}10^{-11}$
	$e + CO_2(X) \rightarrow e + CO(X^1\Sigma_g^+) + O(^1D)$	$f(E/N)$
CO_2 $(X^1\Sigma^+)$	$CO(a^3\Pi) + O_2(X) \rightarrow CO_2(X) + O(^3P)$	$1.2{\cdot}10^{-11}$
	$CO(a^3\Pi) + CO(X^1\Sigma_g^+) \rightarrow CO_2(X) + C(^3P)$	$9.1{\cdot}10^{-13}$
	$O(^3P) + CO(X^1\Sigma_g^+) + CO_2(X^1\Sigma^+) \rightarrow CO_2(X^1\Sigma^+) + CO_2(X^1\Sigma^+)$	$1.6{\cdot}10^{-33}$Exp [-1510/Tg]
	$O(^3P) + CO(X^1\Sigma_g^+) + CO(X^1\Sigma_g^+) \rightarrow CO_2(X^1\Sigma^+) + CO(X^1\Sigma_g^+)$	$8.2{\cdot}10^{-34}$Exp [-1510/Tg]
	$O(^3P) + CO(X^1\Sigma_g^+) + O_2(X^3\Sigma_g^-) \rightarrow CO_2(X^1\Sigma^+) + O_2(X^3\Sigma_g^-)$	$8.2{\cdot}10^{-34}$Exp [-1510/Tg]
	$O^- + CO(X^1\Sigma_g^+) \rightarrow e + CO_2(X^1\Sigma^+)$	$5.8{\cdot}10^{-9}$ $Tg^{-0.39}$

Table 3
Set of main reactions that contribute to the loss of CO_2 $(X^1\Sigma^+)$ and $CO(X^1\Sigma_g^+)$. *f(E/N)* denotes an electron rate coefficient calculated from the Boltzmann equation.

State	Loss	Rate (cm^3/s) or (cm^6/s)
$CO(X^1\Sigma_g^+)$	$e + CO(X^1\Sigma_g^+) \rightarrow e + CO(a^3\Pi)$	$f(E/N)$
CO_2 $(X^1\Sigma^+)$	$e + CO_2(X) \rightarrow e + CO(X^1\Sigma_g^+) + O(^1D)$	$f(E/N)$
	$CO(a^3\Pi) + CO_2(X^1\Sigma^+) \rightarrow 2\,CO(X^1\Sigma_g^+) + CO(X^1\Sigma_g^+)$	$5.0{\cdot}10^{-12}$

towards high values of reduced electric field will take these points into account.

To complete the analysis shown in this section, we further investigated the contribution of the other electronically excited states, namely $O_2(a^1\Delta_g)$, $O_2(b^1\Sigma^+_g)$, $O(^1D)$ on the dissociation fraction of CO_2. To this purpose, additional calculations were performed with an extended version of the model that includes reactions involving $O_2(a^1\Delta_g)$, $O_2(b^1\Sigma^+_g)$, $O(^1D)$, leading to direct production/destruction of new $CO(X^1\Sigma_g^+)$ or CO_2 $(X^1\Sigma^+)$ molecules. In case of O_2 electronically excited states, quantum chemical calculations carried out in [43] showed that reactions like $CO(X^1\Sigma_g^+) + O_2(b^1\Sigma^+_g) \rightarrow CO_2(X^1\Sigma^+) + O(^1D)$ can become relevant for gas temperatures above 1000 K. However, our model shows a negligible contribution of this mechanism due to the typical low gas temperatures considered. As for the $O(^1D)$ state, one can take into account its recombination through $O(^1D) + CO_2(X^1\Sigma^+) \rightarrow CO(X^1\Sigma_g^+) + O_2(X^3\Sigma_g^-)$ with a rate coefficient of $2.4{\cdot}10^{-13}$ cm^3s^{-1} according to [44]. The inclusion of this mechanism contributes to an increase of ~ 0.5 % in the CO_2 dissociation fraction due to the creation of new $CO(X^1\Sigma_g^+)$ molecules. Note that this mechanism also stimulates the production of $O_2(X^3\Sigma_g^-)$, which recombines with $CO(a^3\Pi)$ to form $CO_2(X^1\Sigma^+)$. By considering the reaction $O(^1D) + CO_2(X^1\Sigma^+) \rightarrow CO(X^1\Sigma_g^+) + O_2(X^3\Sigma_g^-)$ we also increase the percentage of $CO_2(X^1\Sigma^+)$ destroyed via neutral mechanisms (about 4%), which leads to the decrease of the relative contribution of electron impact dissociation via $e + CO_2(X^1\Sigma^+) \rightarrow CO(X^1\Sigma_g^+) + O(^1D)$ at steady state. Finally, it is worth noticing that no effect of vibrational excitation on lowering reaction barriers for reactions involving oxygen and CO_2 species was considered. The contribution of $O(^1D)$ to CO_2 dissociation in plasmas where the CO_2 vibrational excitation is significantly higher than in the present conditions is still an open topic of research and requires further investigations.

3.2. Afterglow

To simulate the afterglow regime, we take the concentrations of species obtained during the active phase as input, while setting the electron density and reduced electric field to zero. In principle, this approximation could lead to some inaccuracies in the description of species concentrations, since the electron density can have a decay time within the ms scale. However, one should notice that the EEDF is likely to decay much faster (μs scale). Therefore, and given the reduced electron energy, we expect a small to negligible contribution of electrons on energy threshold-dependent mechanisms during the afterglow. This topic has been addressed in detail in [45]. In this section we consider a gas pressure P = 133.3 Pa and a constant gas temperature T_g = 400 K. Fig. 6 shows the evolution of various species considered in this work. Note that the species concentrations used as input are taken from the values calculated in the previous section at 5 ms. At this point, the input concentrations of $CO(X^1\Sigma_g^+)$ and $O(^3P)$ are nearly the same, while the O_2 $(X^3\Sigma_g^-)$ density is about 2 orders of magnitude lower. We can clearly see that CO_2 $(X^1\Sigma^+)$ and $CO(X^1\Sigma_g^+)$ remain roughly constant throughout the afterglow time, while the concentration of $O_2(X^3\Sigma_g^-)$ starts to increase at about 1 ms as the concentration of $O(^3P)$ decreases. The recombination associated with oxygen species strongly depends on the surface processes and wall recombination probabilities considered in the model. To this purpose, and following [46], we assume a diffusive transport for oxygen species with the following characteristic lifetime:

$$\tau_i = \frac{1}{D_i}\left(\frac{R}{2.405}\right)^2 + \frac{2R(1-\gamma_i/2)}{\gamma_i \langle v_i \rangle} \quad (3)$$

where D_i is the diffusion coefficient of species i, $\langle v_i \rangle$ is its thermal speed, γ_i is its destruction probability on the wall and R is the tube radius. Moreover, and taking into account the Pyrex tube used in the experimental campaign, we assume that atomic oxygen recombines into O_2 according to:

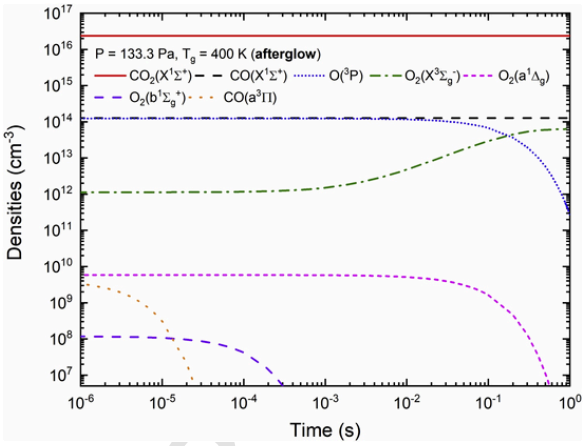

Fig. 6. Calculated concentration of the most important heavy particles as function of the afterglow time, for gas pressure of P = 133.3 Pa, gas temperature of 400 K. Initial species concentrations are taken from values obtained in the discharge pulse (Fig. 3) at 5 ms.

$$O + wall \rightarrow \frac{1}{2}O_2 + wall, \quad (4)$$

with a gas-temperature dependent recombination probability $\gamma_O = 1.8{\cdot}10^{-3}$ Exp [-948/T_g] as measured in [46] for CO_2 discharges. At T_g = 400 K, this gives $\gamma_O \sim 1.7{\cdot}10^{-4}$. Note that the same recombination probability expression is used in the active phase. Such procedure is justified by the experimental measurements from [47] which show a very small difference between the recombination probabilities obtained in the post-discharge and in the plasma exposure in very similar operating conditions. This is in contrast with observations in O_2 plasmas, where the difference can be about 1 order of magnitude [48,49]. In regard to other oxygen species, we follow [50] and consider the recombination probabilities, both in the discharge and afterglow, of $5{\cdot}10^{-4}$, $2{\cdot}10^{-2}$, 1 and 0.1 for $O_2(a^1\Delta_g)$, $O_2(b^1\Sigma^+_g)$, $O(^1D)$ and O_3*, respectively. The decay of the electronic excited oxygen species is illustrated in Fig. 6 through the time evolution of $O_2(a^1\Delta_g)$ and $O_2(b^1\Sigma^+_g)$. To validate the tendencies associated to the decaying of electronic excited oxygen species, we performed additional calculations in pure O_2 and compared the results against the simulations of Marinov et al. [51] and experimental data therein. Finally, it is also worth noticing that due to the lack of electron sources, electron impact excitation becomes negligible, and the concentration of electronic excited states can become strongly reduced for long afterglow times. This is observed in case of the $CO(a^3\Pi)$ state (see Fig. 6), which strongly decays at very short times of the afterglow as a result of the quenching mechanisms given in Tables 2 and 3.

4. Multipulse results

In this section we analyse the influence of different plasma pulses and train configurations on the dissociation fraction of CO_2. Fig. 7 compares experimental data and simulation results for the configuration $t_p^{ON} - t_p^{OFF}$ = 5 – 10 ms ON – OFF time with 10 pulses per train, i.e., N_p = 10. The figure legend follows the notation (N_p x t_p^{ON} - t_p^{OFF} ms). The experimental data was obtained in a glow discharge, sustained at 133.3 Pa with a discharge current of 40 mA [32]. The simulation takes into account the experimental gas pressure and the gas temperature profile (measured in active and afterglow phases), and the reduced electric field of 81.5 Td and electron density $N_e = 7.02{\cdot}10^9$ cm^{-3} (same parameters used in section 3.1). Note that the first points of the dissociation fraction curves correspond to T^{ON} = 5 ms x (N_p = 10) = 0.05 s. Overall, we can see that the model provides a fairly good agreement with the experimental values obtained for the dissociation fraction, de-

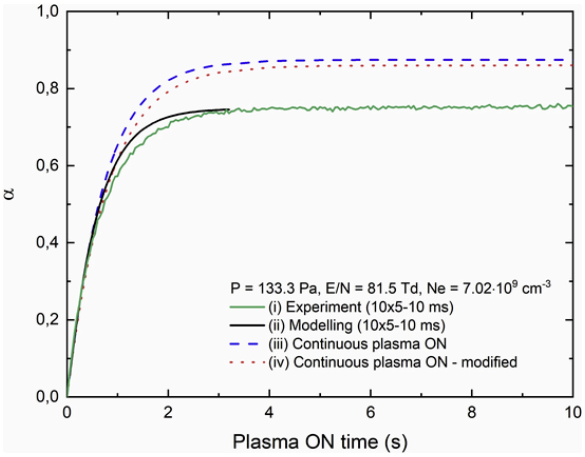

Fig. 7. Time evolution of the dissociation fraction as a function of the total plasma ON time obtained through: (i) experiment at P = 133.3 Pa and 40 mA using glow discharge and $t_p^{ON} - t_p^{OFF}$ = 5–10 ms and N_p = 10 (solid green line), (ii) simulation using $t_p^{ON} - t_p^{OFF}$ = 5–10 ms, N_p = 10, gas pressure P = 133.3 Pa, electron density $N_e = 7.02{\cdot}10^9$ cm^{-3} and reduced electric field E/N = 81.5 Td (solid black line), (iii) simulation assuming a continuous plasma with gas pressure P = 133.3 Pa, electron density $N_e = 7.02{\cdot}10^9$ cm^{-3} and reduced electric field E/N = 81.5 Td (dashed blue line) and (iv) simulation assuming a continuous plasma with modified rate coefficient (by a factor of five) for $CO(a^3\Pi) + CO_2(X^1\Sigma^+) \rightarrow 2CO(X^1\Sigma_g^+) + O(^3P)$ (dotted red line).

scribing very well its initial growth at short plasma ON times and the stabilization around α = 0.75. Note that this dissociation fraction is higher than the values presented in [22] (for similar conditions of pressure and current) due to the absence of gas flow. To further analyse the validity of the model, we analyse the dissociation fraction obtained through continuous plasma operation described in section 3.1, i.e., without pulsed sequence and with a constant gas temperature of 400 K. Note that for the comparison between continuous and pulsed plasma we integrate the plasma ON time of the pulsed sequence. Despite a similar growth of the dissociation fraction for short plasma ON times, the continuous operation leads to a significant increase of the dissociation fraction at the steady-state region. This observation corroborates the experimental evidence indicated in point 1 in section 2.2 and reveals that the decrease of CO_2 dissociation during the OFF time of the plasma pulse is well captured by the model. The individual contributions of different reactions to the evolution of the dissociation fraction in pulsed conditions is further explored in the section below.

Finally, it is worth noticing that some disagreement between experiment and simulation is visible during the transition region (around T^{ON} *= 1 s)*, i.e., between the initial growth and the steady-state region. This can be related to the assumptions considered in the model, namely constant reduced electric field and constant electron energy distribution function throughout the calculations. Naturally, we can also have an overestimation of rate coefficients that contribute to the increase of the dissociation fraction (other than electron impact dissociation). Considering that this disagreement occurs at relatively short times, it is worth analysing reactions with CO_2 as reactant. Fig. 7 contains one additional curve (dotted red line) for the dissociation fraction obtained under continuous operation with a modified rate coefficient for the reaction $CO(a^3\Pi) + CO_2(X^1\Sigma^+) \rightarrow 2CO(X^1\Sigma_g^+) + O(^3P)$, decreasing from $5.0{\cdot}10^{-12}$ cm^{3}s^{-1} to 10^{-12} cm^{3}s^{-1} (see Table 3). This modification is based on set of rate coefficients given in [41] and leads to the decrease of dissociation fraction throughout all the plasma ON time. This example demonstrates the importance of the rate coefficients values used for reactions involving $CO(a^3\Pi)$. However, we should stress that quantitative conclusions relative to the correct value of the rate coefficients are difficult to draw given the large number of variables that influence on the dissociation fraction results. Other reactions related to $CO(a^3\Pi)$ worth investigating in future studies are $CO(a^3\Pi) + O_2(X^3\Sigma_g^-) \rightarrow CO_2(X^1\Sigma^+) + O(^3P)$ and $CO(a^3\Pi) + O_2(X^3\Sigma_g^-) \rightarrow CO(X^1\Sigma_g^+) + 2O(^3P)$, which according to Grigorian et al. [41] have the rates of $6.0{\cdot}10^{-12}$ cm^{3}s^{-1} and $5.0{\cdot}10^{-12}$ cm^{3}s^{-1}, respectively, which represent factors of 0.5 and 0.2 lower than the values used in this work.

4.1. Change of t_p^{OFF}

In this section we present the simulations related to the variation of the OFF time (delay) in-between pulses, t_p^{OFF}, for a fixed ON time. Fig. 8 **(a)** shows the evolution of the dissociation fraction for t_p^{ON} = 5 ms, while t_p^{OFF} takes the values of 1, 5, 10, 50 and 100 ms. The discharge parameters are the same as the ones indicated in the beginning of section 4. We can clearly observe that an increase of t_p^{OFF} leads to a decrease of the dissociation fraction at the steady state region. Moreover, it is also worth noticing that the time t_p^{ON} at which the curves start to diverge is within the range of 0.5–1 s. Both effects were observed experimentally in radio-frequency discharges for pressures of 266.6 and 666.6 Pa, with 40 W of power (see points 2 and 3 in section 2.2). The difference of CO_2 dissociation fractions experimentally obtained at steady state between t_p^{OFF} = 1 ms and t_p^{OFF} = 50 ms is about 0.05, which is within the same order of magnitude observed in the calculations.

To understand the change of the dissociation fraction with t_p^{OFF} we now analyse the contribution of different reactions leading to the creation and loss of $CO_2(X^1\Sigma^+)$ and $CO(X^1\Sigma_g^+)$ for the two extreme cases, i.e., t_p^{OFF} = 1 ms and t_p^{OFF} = 100 ms (see Fig. 8**(b)**). For this analysis we select only mechanisms that lead to an effective production of new CO or CO_2 species. We can see that the reaction $CO(a^3\Pi) + O_2(X^3\Sigma_g^-) \rightarrow CO_2(X^1\Sigma^+) + O(^3P)$ has an increasing contribution with the increase of the t_p^{OFF}, leading to the decrease of the CO_2 dissociation fraction. This observation clearly supports the results found during the steady-state

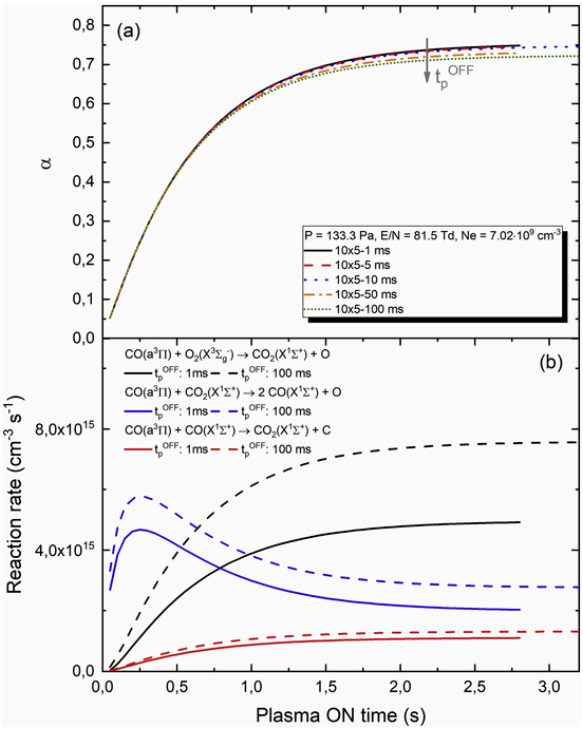

Fig. 8. (a) Time evolution of the dissociation fraction as a function of the total plasma ON time for different delay between pulses t_p^{OFF} with t_p^{ON} = 5 ms, N_p = 10, gas pressure P = 133.3 Pa, electron density $N_e = 7.02{\cdot}10^9$ cm^{-3} and a reduced electric field E/N = 81.5 Td. (b) Reaction contributions of the main creation and loss mechanisms leading to the formation of $CO_2(X^1\Sigma^+)$ and $CO(X^1\Sigma_g^+)$ for t_p^{OFF} = 1 ms and t_p^{OFF} = 100 ms.

region, i.e., an increase of the dissociation fraction with a decrease of t_p^{OFF}. This point also reveals the importance of the recombination of oxygen species during the afterglow. In particular, it is worth noticing that longer OFF times are associated with an increase of $O_2(X^3\Sigma_g^-)$ and decrease of the O (^{3}P) concentration (see Fig. 6) due to O-atom recombination into $O_2(X^3\Sigma_g^-)$. This will then contribute to the decrease of the dissociation fraction of CO_2. Regarding $CO(a^3\Pi) + CO_2(X^1\Sigma^+) \rightarrow 2CO(X^1\Sigma_g^+) + O(^3P)$, we see an increasing contribution for higher t_p^{OFF} values, which should induce higher dissociation fractions. However, the relative contribution between different values of t_p^{OFF} is smaller compared to the first mechanism analysed. It also worth noticing that $CO(a^3\Pi) + CO_2(X^1\Sigma^+) \rightarrow 2CO(X^1\Sigma_g^+) + O(^3P)$ has a decreasing contribution as the plasma ON time increases due to the decrease of $CO_2(X^1\Sigma^+)$ concentration. Finally, the mechanism $CO(a^3\Pi) + CO(X^1\Sigma_g^+) \rightarrow CO_2(X^1\Sigma^+) + C(^3P)$ also reveals an increasing contribution with the increase of the t_p^{OFF}, which also supports the results obtained in Fig. 8**(a)**. Overall, we can deduce that the reactions involving $CO(a^3\Pi)$ with $O_2(X^3\Sigma_g^-)$ and $CO_2(X^1\Sigma^+)$, together with oxygen recombination at the wall reactor, provide good indicators to describe the dissociation fraction trends observed during the steady-state.

4.2. Change of N_p

In this section we analyse the time evolution of the dissociation fraction with the same train configuration of $t_p^{ON} - t_p^{OFF} = 5 - 10$ ms, while changing the number of pulses per train, with $N_p = 2$, 10 and 50 (see Fig. 9). The discharge parameters are the same as the ones indicated in the beginning of section 4. The simulations reveal an increase of the dissociation fraction with the increase of the number of pulses per train N_p. This trend also agrees with the experimental data obtained in radio-frequency discharges for pressure of 266.6 Pa and power of 40 W (see point 4 in section 2.2). Overall, these results reveal a decrease of the dissociation rate due to CO destruction and recombination into CO_2 after the end of each train. Note that the train configuration with $N_p = 2$ case goes through several long "off-times" before reaching the equivalent T^{ON} of the configurations with higher N_p. This leads to an increasing contribution of $CO(a^3\Pi) + O_2(X^3\Sigma_g^-) \rightarrow CO_2(X^1\Sigma^+) + O(^3P)$, which promotes the decrease of the dissociation fraction.

The change of the dissociation fraction with the number of pulses per train N_p (keeping the same $t_p^{ON} - t_p^{OFF}$) observed in calculations is similar to the variation observed in the experimental campaign. Indeed, the experimental difference of dissociation fractions at steady-state between $N_p = 5$ and $N_p = 10$ is about 0.1. A similar order of magnitude is obtained through the simulations by changing N_p. To further analyse

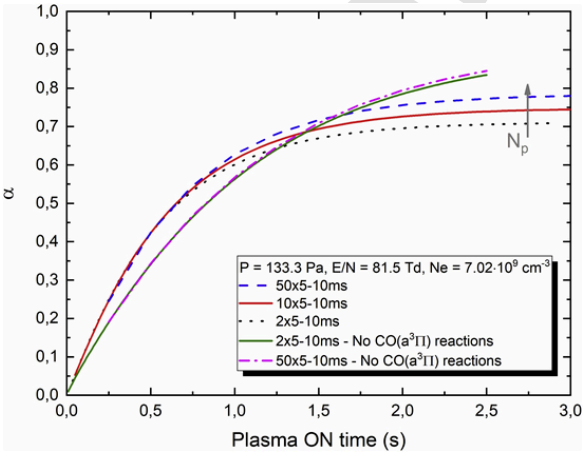

Fig. 9. Time evolution of the dissociation fraction as a function of the total plasma ON time for different values of N_p with the same $t_p^{ON} - t_p^{OFF} = 5$–10 ms, gas pressure P = 133.3 Pa, electron density $N_e = 7.02 \cdot 10^9$ cm^{-3} and a reduced electric field E/N = 81.5 Td.

this point we show two additional dissociation fraction curves corresponding to $N_p = 2$ and $N_p = 50$, without taking into account the reactions involving $CO(a^3\Pi)$. In this case, the $CO_2(X^1\Sigma^+)$ recombination is mainly controlled by $O^- + CO(X^1\Sigma_g^+) \rightarrow e + CO_2(X^1\Sigma^+)$ and three-body reaction mechanisms. Several observations can be made about these results. First, the removal of $CO(a^3\Pi)$ reactions lead to a slower growth of the dissociation fraction. This is a consequence of removing $CO(a^3\Pi) + CO_2(X^1\Sigma^+) \rightarrow 2CO(X^1\Sigma_g^+) + O(^3P)$, which contributes to the production of $CO(X^1\Sigma_g^+)$ for short plasma ON times. At about $T^{ON} = 1$ s, the removal of $CO(a^3\Pi)$ reactions lead to a decrease of the dissociation fraction of about 10 %. Second, the removal of $CO(a^3\Pi)$ reactions leads to longer stabilization times for the CO_2 dissociation fraction. Without $CO(a^3\Pi)$ reactions, the remaining recombination mechanisms depend on atoms and molecules in their ground states, which leads to an increasing contribution of processes with long characteristic times. Finally, the removal of $CO(a^3\Pi)$ reactions also influence the changes observed in the dissociation fraction related to variation of N_p. Indeed, we observe very small difference between modified curves of $N_p = 2$ and $N_p = 50$. Indeed, when these reactions are removed the differences between the curves of $N_p = 2$ and $N_p = 50$ are vanishingly small, in contradiction to the experimental observations.

Overall, the previous points demonstrate once more the importance of considering $CO(a^3\Pi)$ reactions to describe the dissociation fraction in low-pressure discharges. Moreover, this analysis also shows that experiments related to the change of N_p are very suitable to investigate the underlying chemistry of recombination mechanisms in CO_2 discharges. Similar experiments in high-pressure conditions can provide deeper understanding regarding the true nature of 3-body reaction mechanisms. This is of major interest given the large discrepancies in the literature regarding rate coefficients for 3-body reaction mechanisms. Among different rate coefficients found in the literature related to CO_2 plasma-based reforming, it is worth mentioning that some authors consider a negative temperature dependence for the $CO + O + O_2 \rightarrow CO_2 + O_2$ process with the rate coefficient $k(T_g) = 6.51 \cdot 10^{-36} \mathrm{Exp}[+1863/T_g]$ [52]. This negative temperature coefficient is explained by the mechanism

$$O + O_2 \leftrightarrow O_3^{*} \overset{M}{\leftrightarrow} O_3^{**} \overset{CO}{\rightarrow} CO_2 + O_2 \quad (5)$$

where O_3^{**} is a stabilized excited ozone molecule, possibly in the triplet state. Note that at $T_g = 300$ K this expression provides a rate coefficient of $\sim 3.24 \cdot 10^{-33}$ cm^{6}s^{-1}, about 600 times higher than the current value considered in our model (based on the rate coefficient given in [40]). Although this is not very important in the present low-pressure conditions, additional multipulse calculations reveal that the inclusion of a negative temperature dependence provides a more significant variation of the dissociation fraction at steady state due to the change of the number of pulses per train N_p. The effect of exited ozone and the role of 3-body reaction mechanisms should be further investigated in future studies dedicated to CO_2 pulse discharges under high pressure conditions.

4.3. Change of t_p^{ON}

In this final section we analyse the variation of the ON time t_p^{ON} for a fixed OFF time delay between pulses. Fig. 10 shows the evolution of the dissociation fraction for $t_p^{OFF} = 10$ ms, while t_p^{ON} takes the values of 1, 5 and 50 ms. Discharge parameters are the same as the ones indicated in the beginning of section 4. Note that the number of pulses N_p is also modified in order to keep the same period for the pulse trains (0.05 s) in each condition. Overall, the results reveal a small increase of the dissociation fraction at steady-state due to the increase of the pulse duration t_p^{ON}. The increasing tendency agrees with the experimental data obtained in radio-frequency discharges for pressures of 266.6 and 666.6 Pa, with 40 W power (see point 5 in section 2.2). This result was

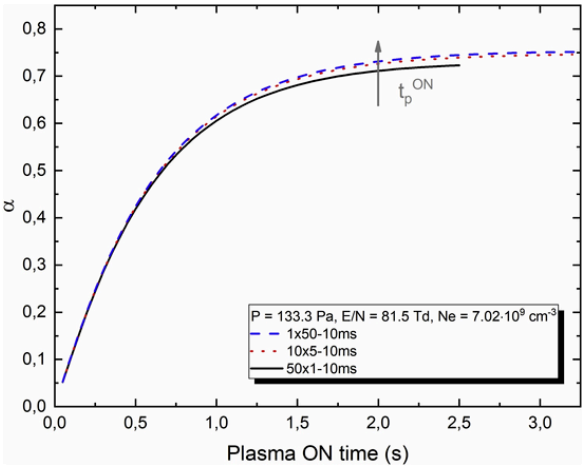

Fig. 10. Time evolution of the dissociation fraction as a function of the total plasma ON time for different delay between pulses t_p^{ON} with t_p^{OFF} = 10 ms, gas pressure P = 133.3 Pa and electron density N_e = 7.02·10⁹ cm⁻³ and a reduced electric field E/N = 81.5 Td.

also expected when considering the importance of reactions involving CO($a^3\Pi$) and oxygen species discussed in the previous section. Note that longer t_p^{ON} times (and corresponding lesser number of pulses N_p) lead to a decrease of O-atom recombination into O_2 ($X^3\Sigma_g^-$) due to the lower number of Off periods per train. This leads to an increase of the CO_2 dissociation fraction given the decrease of the contribution associated with the reaction CO($a^3\Pi$) + O_2 ($X^3\Sigma_g^-$) → CO_2 ($X^1\Sigma^+$) + O (^{3}P).

It is worth noticing that the experimental increase of the dissociation fraction at steady-state due to the change t_p^{ON} is much more significant than what we observe through the simulations. This disagreement can be explained by the lack of detailed input regarding the gas temperature profile. In these simulations we keep the same gas temperature profile, while simply shifting the input time. However, the changes of the t_p^{ON} should also modify the gas temperature growing time which is not taken into account. This point can only be clarified through detailed calculations or measurements of the gas temperature profile during the pulse discharge for different values of t_p^{ON}. At the same time, changes of the t_p^{ON} are likely to be associated to changes of the reduced electric field, electron energy distribution function and electron density. Variations of these parameters will induce different electron impact dissociation rates which may explain the strong experimental changes of the dissociation fraction due to changes of t_p^{ON}.

5. Conclusion

In this work we developed a model to: (i) describe the time evolution of plasma species, (ii) study the relative importance of different mechanisms and (iii) investigate the temporal evolution of the dissociation fraction in CO_2 pulsed discharges, under low pressure conditions. Capitalizing on the *building-up experiments* carried in pulsed DC glow discharges and radio-frequency discharges, we analysed the CO_2 dissociation fraction and the influence of different mechanisms involving electronic excited states. The model was used to analyse the experimental trends associated with different pulsed configurations, namely related to the pulse duration and delay between pulses. The simulations validated the chemical module proposed for CO_2 plasmas and revealed the importance of back reactions involving the CO($a^3\Pi$) states and oxygen species relaxation during the afterglow for the understanding of the CO_2 chemistry. In particular, it was shown that in low-pressure pulsed plasmas the kinetics of CO_2 ($X^1\Sigma^+$), CO($X^1\Sigma_g^+$), + CO($a^3\Pi$), O_2 ($X^3\Sigma_g^-$) and O(^{3}P) are strongly coupled, via (in temporal order) e + CO($X^1\Sigma_g^+$) ↔ e + CO($a^3\Pi$), CO($a^3\Pi$) + CO_2 ($X^1\Sigma^+$) → 2 CO($X^1\Sigma_g^+$) + O(^{3}P), O(^{3}P) + wall → ½ O_2 ($X^3\Sigma_g^-$) and CO($a^3\Pi$) + O_2 ($X^3\Sigma_g^-$) → CO_2 ($X^1\Sigma^+$) + O(^{3}P). These reactions can explain the complex and rich behaviour of the CO_2 dissociation fraction observed experimentally [32,33]. These results are particularly relevant for future applications involving CO_2 discharges under low pressure-conditions (e.g., *in-situ* research utilization for oxygen production on Mars).

We also discussed several limitations associated to the model, while pointing towards several directions of future investigations. First, in regard to the electron kinetics, next studies need to take into account time-resolved electric field and time-dependent electron energy distribution functions, which can be taken into account with quasi-stationary approaches to solve the electron Boltzmann equation in CO_2 pulsed plasmas [36]. Second, in order to improve the chemistry module used in this work, future studies need to deeply address reaction mechanisms involving CO_2 and electronically excited states, namely $O_2(a^1\Delta_g)$, $O_2(b^1\Sigma_g^+)$ and O(^{1}D). The latter species is preferentially formed in CO_2 dissociation by direct electron impact and its role in the overall plasma chemistry and in mediating vibrational energy transfers is still poorly known. Finally, future studies shall address the nature of three-body reactions to properly describe the recombination of CO_2 at high pressure conditions of interest for plasma reforming.

Author statement

Tiago Silva: Conceptualization, Methodology, Software, Formal Analysis, Writing – Original Draft, Visualization.

Ana Sofia Morillo-Candas: Investigation.

Olivier Guaitella: Investigation.

Vasco Guerra: Writing – Review & Editing.

Declaration of Competing Interest

The authors report no declarations of interest.

Acknowledgements

This work was supported by the Portuguese FCT – Fundação para a Ciência e a Tecnologia, under the projects UIDB/50010/2020, UIDP/50010/2020 and the individual grant of Scientific Employment Stimulus (CEECIND/00010/2018). ASMC was funded by LabEx Plas@par receiving finnancial aid from the French National Research Agency (ANR) under project SYCAMORE, reference ANR-16-CE06-0005-01.

References

[1] H.L. van Soest, M.G.J. den Elzen, D.P. van Vuuren, Nat. Commun. 12 (2021) 2140.
[2] A.P.H. Goede, R. Van de Sanden, Europhys. News 47/3 (2016) 22–26.
[3] A. Fridman, Plasma Chemistry, Cambridge University Press, 2008.
[4] G.J. van Rooij, D.C.M. van den Bekerom, N. den Harder, T. Minea, G. Berden, W.A. Bongers, R. Engeln, M.F. Graswinckel, E. Zoethout, M.C.M. van de Sanden, Faraday Discuss. 183 (2015) 233–248.
[5] A.J. Wolf, T.W.H. Righart, F.J.J. Peeters, W.A. Bongers, M.C.M. van de Sanden, Plasma Sources Sci. Technol. 29 (2020) 025005.
[6] C. Montesano, M. Faedda, L.M. Martini, G. Dilecce, P. Tosi, J. Co2 Util. 49 (2021) 101556.
[7] S. Li, M. Ongis, G. Manzolini, F. Galluci, Chem. Eng. J. 410 (2021) 128335.
[8] D.J. Dinh, G. Trenchev, D.H. Lee, A. Bogaerts, J. Co2 Util. 42 (2020) 101352.
[9] A. Bogaerts, E.C. Neyts, ACS Energy Lett. 3 (2018) 1013–1027.
[10] L.D. Pietanza, et al., Eur. Phys. J. D. (2021), Accepted for publication.
[11] A.J. Wolf, F.J.J. Peeters, P.W.C. Groen, W.A. Bongers, M.C.M. van de Sanden, J. Phys. Chem. C 124 (2020) 16806–16819.
[12] G. Chen, R. Snyders, N. Britun, J. Co2 Util. (2021), Accepted for publication.
[13] G. Chen, F. Buck, I. Kistner, M. Widenmeyer, T. Schiestel, A. Schulz, M. Walker, A. Weidenkaff, Chem. Eng. J. 392 (2020) 123699.
[14] A.P.H. Goede, EPJ Web of Conferences, 189, 2018, p. 10.
[15] G.J. Van Rooij, H.N. Akse, W.A. Bongers, M.C.M. Van De Sanden, Plasma Phys. Control. Fusion 60 (2018) 014019.
[16] M. Grofulovic, L.L. Alves, V. Guerra, J. Phys. D Appl. Phys. 49 (2016) 395207.
[17] P. Ogloblina, A. Tejero-del-Caz, V. Guerra, L.L. Alves, Plasma Sources Sci. Technol. 29 (2020) 15002.
[18] T. Silva, M. Grofulovic, B.L.M. Klarenaar, A.S. Morillo-Candas, O. Guaitella, R. Engeln, C.D. Pintassilgo, V. Guerra, Plasma Sources Sci. Technol. 29 (2018) 15019.
[19] M. Grofulovic, T. Silva, B.L.M. Klarenaar, A.S. Morillo-Candas, O. Guaitella, R. Engeln, C.D. Pintassilgo, V. Guerra, Plasma Sources Sci. Technol. 29 (2018) 115009.
[20] L. Terraz, T. Silva, A.S. Morillo-Candas, O. Guaitella, A. Tejero-del-Caz, L.L. Alves, V. Guerra, J. Phys. D Appl. Phys. 53 (2019) 094002.

[21] T. Silva, M. Grofulovic, L. Terraz, C.D. Pintassilgo, V. Guerra, Plasma Process 40 (2020) 713–725.
[22] A.F. Silva, A.S. Morillo-Candas, A. Tejero-del-Caz, L.L. Alves, O. Guaitella, V. Guerra, Plasma Sources Sci. Technol. 29 (2020) 125020.
[23] P. Ogloblina, A.S. Morillo-Candas, A.F. Silva, T. Silva, A. Tejero-del-Caz, L.L. Alves, O. Guaitella, V. Guerra, Plasma Sources Sci. Technol. 30 (2021) 065005.
[24] V. Guerra, T. Silva, P. Ogloblina, M. Grofulovic, L. Terraz, M.L. da Silva, C.D. Pintassilgo, L.L. Alves, O. Guaitella, Plasma Sources Sci. Technol. 26 (2017) 11LT01.
[25] B.L.M. Klarenaar, R. Engeln, D.C.M. van den Bekerom, M.C.M. van de Sanden, A.S. Morillo-Candas, O. Guaitella, Plasma Sources Sci. Technol. 26 (2017) 115008.
[26] T. Dias Atomic Oxygen Kinetics in CO2 Plasmas MSc thesis Retrieved from Instituto Superior Técnico https://fenix.tecnico.ulisboa.pt/cursos/meft/dissertacao/846778572212336 2019
[27] T. Kozák, A. Bogaerts, Plasma Sources Sci. Technol. 23 (2014) 045004.
[28] T. Kozák, A. Bogaerts, Plasma Sources Sci. Technol. 23 (2015) 015024.
[29] M. Capitelli, G. Collona, G.D. Ammando, L.D. Pietanza, Plasma Sources Sci. Technol. 26 (2017) 1–17.
[30] D.R. Harding, R.E. Weston Jr., G.W. Flynn, J. Chem. Phys. 88 (1988) 3590.
[31] H. Chen, H. Chiang, H. Matsui, S. Tsuchiya, Y. Lee, J. Phys. Chem. A 113 (2009) 3431–3437.
[32] A.S. Morillo-Candas, T. Silva, B.L.M. Klarenaar, M. Grofulovic, V. Guerra, O. Guaitella, Plasma Sources Sci. Technol. 29 (2020) 01LT01.
[33] A.S. Morillo-Candas, V. Guerra, O. Guaitella, J. Phys. Chem. C 124 (2020) 17459–17475.
[34] N. Yu Babaeva, G.V. Naidis, Plasma Sources Sci. Technol. 30 (2021) 03LT03.
[35] A. Tejero-del-Caz, V. Guerra, D. Gonçalves, M.L. da Silva, N. Pinhão, C.D. Pintassilgo, L.L. Alves, Plasma Sources Sci. Technol. 28 (2019) 043001.
[36] A. Tejero-del-Caz, V. Guerra, N. Pinhão, C.D. Pintassilgo, L.L. Alves, Plasma Sources Sci. Technol. 30 (2021) 065008.
[37] G. Gousset, C.M. Ferreira, M. Pinheiro, P.A. Sa, M. Touzeau, M. Vialle, J. Loureiro, J. Phys. D Appl. Phys. 24 (1991) 290–300.
[38] L.L. Alves, P. Coche, M.A. Ridenti, V. Guerra, Eur. Phys. J. D 70 (2016) 124.
[39] L.D. Pietanza, G. Colonna, M. Capitelli, Phys. Plasmas 27 (2020) 23513.
[40] A. Cenian, A. Chernukho, V. Borodin, G. Sliwinski, Contr. Plasma Phys. 34 (1994) 25–37.
[41] G.M. Grigorian, I.V. Kochetov, Plasma Phys. Rep. 30 (2004) 788–796.
[42] L.D. Pietanza, G. Colonna, M. Capitelli, Front. Chem. 7 (2019) 1–14.
[43] A. Sharipov, A. Starik, J. Phys. Chem. A 115 (2011) 1795–1803.
[44] M.J. Perri, A.L. van Wyngarden, K.A. Boering, J.J. Lin, Y.T. Lee, J. Chem. Phys. 119 (2003) 8213–8216.
[45] V. Guerra, P.A. Sá, J. Loureiro, Phys. Rev. 63 (2001) 046404.
[46] A.S. Morillo-Candas, C. Drag, J.P. Booth, T.C. Dias, V. Guerra, O. Guaitella, Plasma Sources Sci. Technol. 28 (2019) 075010.
[47] A.S. Morillo-Candas, Investigation of Fundamental Mechanisms of CO_2 Plasmas, Ph.D thesis. Laboratoire de Physique des Plasmas (LPP), Ecole Polytechnique, 2019.
[48] L. Magne, H. Coitout, G. Cernogora, G. Gousset, J. Phys. III 3 (1993) 1871–1889.
[49] G. Cartry, L. Magne, G. Cernogora, J. Phys. D Appl. Phys. 33 (2000) 1303.
[50] A. Annusová, D. Marinov, J.P. Booth, N. Sirse, M.L. da Silva, B. Lopez, V. Guerra, Plasma Sources Sci. Technol. 27 (2018) 045006.
[51] D. Marinov, V. Guerra, O. Guaitella, J.P. Booth, A. Rousseau, Plasma Sources Sci. Technol. 22 (2013) 055018.
[52] V.N. Kondratiev, Reac. Kinet. Catal. Lett. 1 (1974) 7–13.